Journal of Colloid and Interface Science 324 (2008) 47–54

Contents lists available at ScienceDirect

Journal of Colloid and Interface Science

www.elsevier.com/locate/jcis

# Dual-stimuli responsive PNiPAM microgel achieved *via* layer-by-layer assembly: Magnetic and thermoresponsive

John E. Wong [a,*], Akhilesh K. Gaharwar [a,b], Detlef Müller-Schulte [c], Dhirendra Bahadur [b], Walter Richtering [a]

[a] *RWTH Aachen University, Institute of Physical Chemistry, Landoltweg 2, 52056 Aachen, Germany*
[b] *Indian Institute of Technology-Bombay, Department of Metallurgical Engineering and Materials Science, Mumbai, India*
[c] *MicroCoat GmbH, Martelenberger Weg 8, 52066 Aachen, Germany*

ARTICLE INFO

*Article history:*
Received 18 January 2008
Accepted 13 May 2008
Available online 17 May 2008

*Keywords:*
Magnetic nanoparticles
Microgels
Layer-by-layer
Polyelectrolytes
Hybrid core–shell

ABSTRACT

We describe the synthesis, characterisation and surface-modification of magnetic nanoparticles and a poly(*N*-isopropylacrylamide) microgel, followed by the assembly and characterisation of magnetic nanoparticles on the microgel. To facilitate this deposition, the surface of the microgel is first modified *via* the layer-by-layer assembly of polyelectrolytes. One advantage of this concept is that it allows an independent optimization and fine tuning of the magnetic and thermoresponsive properties of individual components (nanoparticles and microgels) before assembling them so that the hybrid core–shell structure retains all the individual properties. The decisive parameter when exploiting the thermoresponsive and magnetic properties in such hybrid core–shell structures is the amount of heat transfer from the magnetic core onto the thermosensitive (loaded) microgel (for the subsequent heat-triggered release of drugs). Inductive heat study reveals that the heat generated by the magnetic nanoparticles is sufficient to cause the collapse of the microgel above its volume phase transition temperature. Successful confinement of positively and negatively charged magnetic nanoparticles between polyelectrolyte layers is achieved using the layer-by-layer deposition onto the microgel. Dynamic light scattering measurements show (i) the presence of each layer successfully deposited, (ii) the preservation of thermoresponsivity in the coated microgel, and (iii) that the magnetic nanoparticles do not get detached during the phase transition of the microgel. Electrophoresis measurements confirm charge reversal at every stage of layering of polycations, polyanions and magnetic nanoparticles. This unique combination of thermoresponsivity and magnetism opens up novel perspectives towards remotely controlled drug carriers.



## 1. Introduction

Much effort has been devoted to the synthesis of organic/inorganic nanocomposites [1–6] in an attempt to exploit new hybrid properties derived from the various components. Because of their small size, nanoparticles (NP) offer unique properties and magnetic nanoparticles (MNP) based on iron oxide composites or hybrid materials, essentially in the form of core–shell systems are finding great interest in the field of biomedical applications [7–12]. For *in vivo* applications of MNP, three basic prerequisites have to be met: (i) the surface has to be biocompatible, (ii) non-toxic, and (iii) the particles must be well-dispersed without forming aggregates. Ideally, surface modification should provide good colloidal stability [1,6], biocompatibility and chemical functionality for the potential attachment of biorecognisable ligands. From this has stemmed the idea of using a magnetic core encapsulated in a protective shell. One rational approach is to embed nanoparticles in silica since the latter can be readily functionalised to impart the protective shell [13,14]. We recently reported the *in situ* as well as the post-modification of MNP with polyelectrolytes, without the need for encapsulation in silica [15,16].

One of the numerous applications of MNP in medicine is cancer treatment [17,18]. Hyperthermia is a promising approach to cancer therapy [19–21]. MNP can be used to target specific tumor tissue, and cancer-specific hyperthermia may be achieved by applying an external alternating current (ac) magnetic field whereby causing MNP to generate heat by inductive heating and increase the temperature to 41–46 °C to kill tumor cells [19–21]. By combining the magnetic property of MNP with the thermoresponsive property of some polymers one can achieve dual-stimuli hybrid core–shell structures. Thermoresponsive magnetic polymer particles are particularly attractive for drug delivery [22–24]. Thermoresponsive microgels have the unique property of undergoing a reversible phase transition. Thermoresponsive microgels (i) have high surface-to-volume ratios, and hence high drug-loading capacities, and (ii) undergo fast, reversible structural changes from a swollen to a collapsed state by expulsing the solvent, therefore

* Corresponding author. Fax: +49 241 8092327.
*E-mail address:* wong@pc.rwth-aachen.de (J.E. Wong).

0021-9797/$ – see front matter 
doi:10.1016/j.jcis.2008.05.024

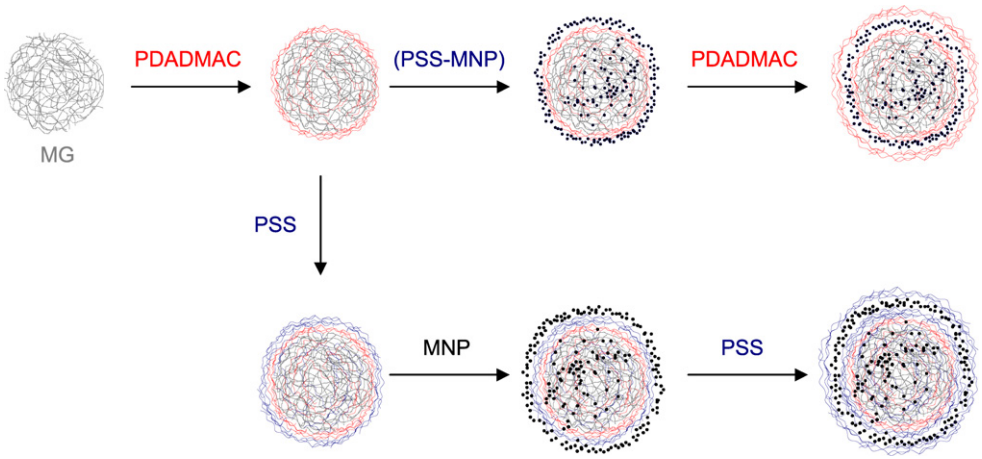


**Scheme 1.** Simplistic representation of the LbL assembly of polyelectrolytes, unmodified and modified magnetic nanoparticles on microgels.

possess a release-trigger mechanism, making them potential candidates as remote-controlled drug delivery vehicles [22]. One of the most widely studied microgels is poly(*N*-isopropylacrylamide) (PNiPAM) [25]. It is non-hazardous, soluble in water, and possesses a volume phase transition temperature (VPTT) around 32 °C, at which temperature it undergoes a transition from a swollen hydrophilic to a collapsed hydrophobic state. This means that above 32 °C PNiPAM releases most of its water content so that a pronounced shrinking is simultaneously observed. This simultaneous shrinking and water release of PNiPAM could be exploited for drug storage, transport and release. If (drug-loaded) PNiPAM is to be used *in vivo*, one has to devise a means to remotely heat the microgel above its VPTT to release the drug. One way is to incorporate MNP in/on the microgel and use an external magnetic field as a "trigger" to inductively generate enough *in situ* heat to cause the microgel to shrink [15].

To realise such a core–shell structure, one can employ the layer-by-layer (LbL) assembly devised by Decher et al. in the early 1990s [26,27]. The LbL is a very simple, versatile and elegant technique which involves the sequential adsorption of polycations and polyanions on any charged surface, irrespective of shape and size. Polyelectrolyte multilayers (PEM) as well as NP have been successfully deposited on thermoresponsive microgels [15,28–33]. The rational behind this core–shell structure is that the thickness (number of layers) and porosity (nature of polyelectrolyte pair and of the assembly conditions) of polyelectrolyte shells assembled around the (loaded) microgel provide barrier properties for regulating molecules trafficking for controlled release, while MNP incorporated within that shell will provide the inductive heat (with the help of an external magnetic field) to cause the collapse of the microgel and acts as a trigger mechanism to release the drug.

In this work, we report the LbL assembly of PEM as well as MNP as a shell on a thermoresponsive PNiPAM core (see Scheme 1). One advantage of this concept is that it allows the independent optimization and fine tuning of the magnetic and thermoresponsive properties of individual components (nanoparticles and microgels) before assembling them with the hope that the resulting hybrid core–shell structure retains all the individual properties. We previously reported such a hybrid core–shell structure; however, charge reversal was not successful after the deposition of MNP [15]. For this work, we choose a PNiPAM with a different swelling ratio in combination with both positively as well as negatively charged MNP. We report successful charge reversal after deposition of each charged species, which enables the deposition of an additional outermost layer of the oppositely charged polyelectrolyte to confine the MNP within the shell. This hybrid core–shell microgel offers a unique combination of thermoresponsivity and magnetism that could open up novel prospects for remotely controlled drug carriers. We describe first the synthesis and characterisation of the MNP, then those of the PNiPAM, and finally those of the hybrid core–shell structures.

## 2. Experimental

### 2.1. Materials

Ferrous chloride tetrahydrate ($FeCl_2{\cdot}4H_2O$), ferric chloride hexahydrate ($FeCl_3{\cdot}6H_2O$), 25% ammonium hydroxide solution, 37% hydrochloric acid (HCl) solution, poly(sodium 4-styrenesulfonate) (PSS, MW = 70 kg mol$^{-1}$), poly(diallyldimethylammonium chloride) (PDADMAC, MW = 100–200 kg mol$^{-1}$) and *N*-isopropylacrylamide (NiPAM) were purchased from Sigma-Aldrich. *N*,*N*′-methylene-bis(acrylamide) (BIS) and sodium dodecyl sulfate (SDS) were purchased from Fluka. Potassium peroxodisulfate (KPS) was purchased from Merck. All chemicals from commercial origin were used without purification. Water was ion-exchanged to a specific resistance of $\rho \geqslant 18$ MΩ cm (Milli-Q) and then double-distilled. The polyelectrolytes were dissolved in water at a concentration of 1 g L$^{-1}$ and used as such with no further adjustment of the pH.

### 2.2. Synthesis of MNP

MNP were prepared according to a co-precipitation technique [34] previously described with a slight modification [15]. Briefly, a $Fe^{3+}$ solution was prepared by dissolving 4.86 g $FeCl_3{\cdot}6H_2O$ in 30 ml distilled water and a $Fe^{2+}$ solution was prepared by dissolving 2.98 g $FeCl_2{\cdot}4H_2O$ in a mixture of 10 ml water and 1.5 ml 37% HCl. Both solutions were placed in an ultrasonic bath for 5 min to homogenize the mixture. The $Fe^{3+}$ and $Fe^{2+}$ solutions were then mixed and allowed to stand in the ultrasonic bath for a short time (about 2 min) just before the precipitation step. To precipitate the iron oxide, the resulting mixture of $Fe^{3+}$ and $Fe^{2+}$ was added drop-wise to a flask containing 240 ml water and 60 ml of 25% $NH_3$ under vigorous stirring (500 rpm). A black suspension was formed immediately and MNP formation was allowed to proceed for 30 min at room temperature with constant stirring to produce a stable, water-based suspension. Aggregates were first separated from the reaction mixture using a strong magnet, and then washed three times with 0.3 M $NH_3$ solution. The washed precipitate was peptized by washing twice with 60 ml of 2 M $HNO_3$ solution. Three cycles of centrifugation at 5000 rpm for 10 min were done and the precipitate dissolved in 120 ml of double-distilled water to give a stable ferrofluid. This unmodified MNP is positively charged.

### 2.3. Synthesis of PSS-modified MNP

Briefly the same procedure was followed with 0.81 g $FeCl_3 \cdot 6H_2O$ in 5 ml distilled water and 0.49 g $FeCl_2 \cdot 4H_2O$ in a mixture of 1 ml water and 0.25 ml 37% HCl. However to precipitate the iron oxide, the mixture of $Fe^{3+}$ and $Fe^{2+}$ was added drop-wise to a three-necked round bottom flask now containing a mixture of 0.1 g of PSS in 40 ml of water and 10 ml of 25% $NH_3$ solution under vigorous stirring (500 rpm) condition. Purification stages were similar (as described above) except that now three cycles of centrifugation at 10000 rpm for 10 min were used and the precipitate dispersed in 20 ml of double-distilled water to get a stable ferrofluid. This PSS-modified MNP, denoted in the text as (PSS-MNP), is negatively charged.

### 2.4. Synthesis of PNiPAM microgel

The synthesis of PNiPAM microgel *via* free radical dispersion polymerisation has been reported elsewhere [35,36]. Briefly, 68.86 g *N*-isopropyl-acrylamide (NiPAM), 1.313 g *N*,*N*′-methylene-bis(acrylamide) (BIS), and 1.313 g sodium dodecyl sulfate (SDS) were dissolved in 4000 ml water at 72 °C under an inert atmosphere of nitrogen at 300 rpm. 3.5 g potassium persulfate (KPS) was dissolved in 50 ml of water and added to the reaction vessel to start the reaction. The reaction was continued for another 5 h under nitrogen. The reaction mixture was passed through glass wool in order to remove particulate matter and further purified by three centrifugation cycles (30, 20, and 15 min) using a Sorvall Discovery$^{TM}$ 90SE ultracentrifuge, with removal of the supernatant and redispersion between each cycle. The microgel was finally collected, redispersed in water overnight, and filtered through a 1.2 μm filter.

### 2.5. LbL of PEM on PNiPAM microgel

The surface modification of the PNiPAM was carried out using the LbL technique to deposit PEM [28,30,32] (see Scheme 1). PNiPAM (MG) is negatively charged, and consequently, the first coating is accomplished by the deposition of a PDADMAC layer. Briefly, 10 ml of a 1:100 diluted dispersion of microgel were added to 20 ml of an aqueous solution of 1 mg ml$^{-1}$ PDADMAC solution and mixed for 24 h. The excess polyelectrolyte was removed by ultracentrifugation at 50 000 rpm for 30 min at 25 °C, and the PDADMAC-coated microgel (MG/PDADMAC) washed by redispersion in water. The washing, redispersion and centrifugation steps were repeated three times to ensure removal of loosely bound PDADMAC. The MG/PDADMAC obtained was finally redispersed in water overnight and filtered through a 1.2 μm filter. MG/PDADMAC constitutes the main precursor for further build-up of either PEM or (PSS-MNP). In order to deposit positively charged MNP, a negatively charged surface is needed, and this is achieved by depositing a layer of polyanion such as PSS to obtain MG/PDADMAC/PSS. To add a layer of PSS on MG/PDADMAC, the above-mentioned procedure is employed.

### 2.6. LbL of MNP on surface-modified PNiPAM

Positively charged MNP were added to PSS-terminated surface-modified microgel, MG/PDADMAC/PSS while negatively charged (PSS-MNP) were added to PDADMAC-terminated surface-modified microgel, MG/PDADMAC [15], as illustrated in Scheme 1. Briefly, to deposit the MNP on the polyelectrolyte-coated microgel, a solution of the oppositely charged surface-modified microgel was added slowly to a dilute solution of MNP in a volume ratio of 1:5 and mixed for 24 h. The microgel coated with MNP was separated from excess MNP by magnetic separation. We observed that MNP are very stable and do not form agglomeration in the presence of a magnetic field. However, when microgels coated with (PSS-MNP) are exposed to a magnetic field, these particles are then attracted to the magnet very fast due to the higher magnetic dipole interaction between the MNP present on the microgel. The MNP-coated microgels, MG/PDADMAC/PSS/MNP and MG/PDADMAC/(PSS-MNP), were then washed 3 times with water by using the above-mentioned procedure at 25 °C, and finally redispersed in water overnight. To confine the MNP onto the microgel, one or two layers of polyelectrolyte were deposited on the MNP-coated microgel using the procedure mentioned above.

### 2.7. Characterisation

X-ray diffraction (XRD) of the MNP was performed on a Philips X'pert Diffractometer, PW 3040/60 system using Cu$K_\alpha$ radiation ($\lambda = 0.1541$ nm). XRD graphics were compared to the JCPDS standard data in order to deduce the crystal structure of the product. The crystallite size was determined from the X-ray line broadening using Scherrer's formula. Thermogravimetric analysis (TGA) was carried out on the dried samples with a heating rate of 10 °C min$^{-1}$ (from 20 to 600 °C), using a DuPont 9900 thermogravimetric analyser in a nitrogen atmosphere. Fourier transform infrared (FTIR) spectra were recorded on a Nicolet Magna 550 spectrometer within the wave range of 4000–400 cm$^{-1}$. For FTIR analysis, an aqueous solution of the MNP was dried in an oven at 80 °C and the powder samples were palletized with dried KBr. Magnetic properties of the particles were measured by Vibrating Sample Magnetometer (VSM) (Lake Shore, Model 7410) while zero-field cooled (ZFC) and field-cooled (FC) magnetisation data (in the range of 5–300 K) were obtained from a SQUID magnetometer (MPMS-5S, Quantum Design, San Diego, USA). Transmission Electron Microscope (TEM) images of particles directly deposited on a carbon-coated grid were taken on a Philips, CM200 microscope working at 200 kV. Inductive heating was performed using a generator–oscillator-combination (TIG 5/300, Hüttinger, Freiburg, Germany) operated at maximum output: power 5.2 kW; current 26.5 A and a frequency of 200 kHz. Under these conditions a maximum magnetic field amplitude of 3.8 kA m$^{-1}$ was calculated at the centre of the coil. A Varian SpectrAA-50B Atomic Absorption Spectrometer was used to determine the iron concentration. Dynamic light scattering (DLS) experiments were carried out on highly diluted samples with an ALV goniometer equipped with an avalanche photodiode and a temperature-controlled cell compartment to determine the hydrodynamic diameter, $D_h$. The samples were allowed to equilibrate for 20 min before a reading was taken, and three sets of recordings were measured at each temperature. Temperature was varied from 20 to 60 °C, in steps of 2 °C, in both directions, so that one complete cycle consists of a heating curve followed by a cooling curve. Scattered light was detected at 60° with an integration of 120 s and computed with a digital ALV 5000E auto-correlator using an ALV Software version 5.3.2. Particles size was calculated by cumulant fits. The zeta potential ($\zeta$-potential) and the electrophoretic mobility ($\mu$) were determined using a Zetasizer 3000HSA (from Malvern Instruments, England) as a function of the number of layers. Each point is the average of at least ten consistent measurements.

## 3. Results and discussion

### 3.1. MNP characterisation

Fig. 1a shows the XRD analysis carried out on both the native MNP and the modified one, (PSS-MNP). The same characteristic peaks of magnetite or maghemite ($2\theta \sim 34.9°$, 41.2°, 50.3°, 67.1° and 74.3°), marked, respectively, by their indices ((220), (311),

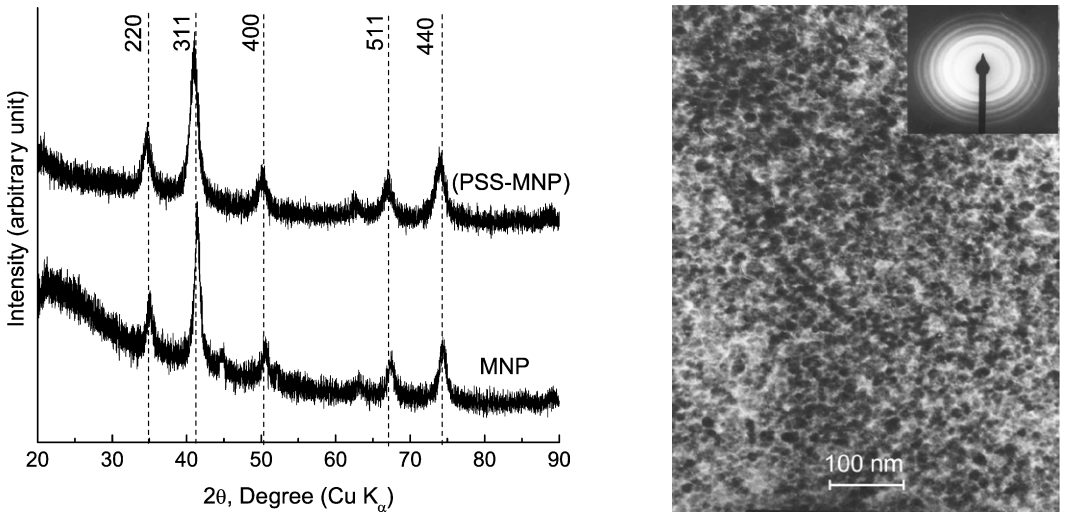


**Fig. 1.** (a) XRD patterns of MNP and (PSS-MNP) with characteristic peaks at $2\theta \sim 35°$, 41°, 50°, 67° and 74° confirm the presence of magnetite or maghemite. Vertical dotted line is only a guide to the eye. (b) TEM image shows (PSS-MNP) particles with a number-average size around 5 nm. The electron diffraction pattern is shown in the inset.

(400), (511) and (440)), were observed for both samples [15]. The peaks were significantly broadened due to the small size of the crystallites. The volume average relative particle size of the crystal, $D$, was calculated using the Scherrer formula giving $D_{311}$ (MNP) ∼7 nm and $D_{311}$ (PSS-MNP) ∼5 nm. No additional peak, after surface modification with PSS, suggests that the coating does not result in any phase change of the MNP. The decrease in crystallite size shows that PSS is effective to make smaller crystallites by controlling the nucleation and growth process.

TEM picture in Fig. 1b shows that the (PSS-MNP) is somewhat irregularly shaped from oval to spherical, nearly monodisperse and the number-average particle size is estimated around 5 nm (compared to around 7 nm for the MNP), which is typical for monodomains of superparamagnetic iron oxide nanoparticles [8]. There is an excellent agreement between crystallite size obtained from X-ray line broadening and TEM results. The inset of Fig. 1b shows the electron diffraction pattern of (PSS-MNP) which consists of concentric rings consistent with a cubic inverse spinel structure of magnetite. The electron diffraction pattern of MNP is similar. The characteristic d spacing corresponds to the $hkl$ value (220), (311), (400), (422), (511), (440) and (533). These results show excellent agreement with the XRD data.

The surface modification of MNP with PSS was confirmed by electrophoretic measurements ($\zeta$-potential and $\mu$). MNP has a $\zeta$-potential and a $\mu$ of +20 mV and $+1.55 \times 10^{-8}$ $m^2\,V^{-1}\,s^{-1}$, respectively. The net positive surface charge on the MNP is due to the peptization of the surface. When MNP are prepared *in situ* in the presence of PSS, the resulting particles (PSS-MNP) have now a $\zeta$-potential and a $\mu$ equal to −30 mV and $-2.15 \times 10^{-8}$ $m^2\,V^{-1}\,s^{-1}$, respectively [16]. The negative surface charge is due to negatively charged sulfonate groups of the PSS indicating that the PSS is indeed bound to the MNP. The $D_h$ of (PSS-MNP) is 55 nm compared to 30 nm for the unmodified MNP; these values could indicate some aggregations. Although both samples show narrow polydispersity, the narrower size distribution of (PSS-MNP) (data not shown) shows that PSS is somehow effective to produce monodisperse particles. No agglomeration is observed from the DLS study. The increase in $D_h$ of (PSS-MNP) as compared to MNP is consistent with the presence of the polyelectrolyte which can form tails and loops around the MNP core.

Further evidence of the presence of the polyelectrolyte bound to the MNP is provided by FTIR spectra as shown for MNP and (PSS-MNP) in Fig. 2. For as prepared MNP, the broad absorption band

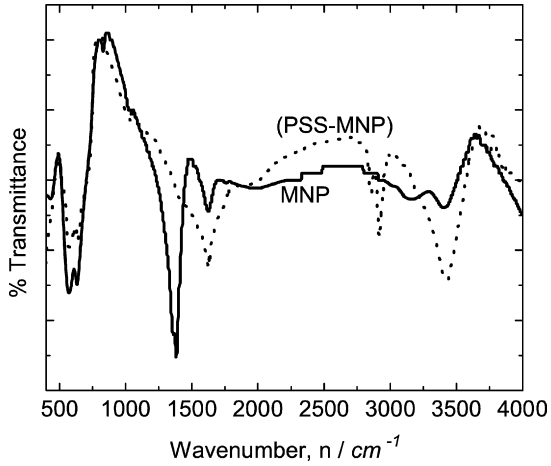


**Fig. 2.** FTIR spectra of positively charged MNP and negatively charged (PSS-MNP) provide evidence of the polyelectrolyte bound to the MNP. Additional peaks at 2930 and 2854 $cm^{-1}$, and decrease in intensity at 588, 680 and 1380 $cm^{-1}$ supports the presence of PSS on (PSS-MNP) particles.

between 3000 and 3600 $cm^{-1}$ (with peak at around 3404 $cm^{-1}$) and the band at 1620 $cm^{-1}$ are associated with the fundamental valence stretching vibrations of the $H_2O$; the band at 1385 $cm^{-1}$ is due to bending modes of O–C–H, C–C–H, and C–O–H angles of carbonate present on the surface of the MNP (as reaction was done in ambient conditions); and bands at 568 and 644 $cm^{-1}$ are due to the stretching vibration of Fe–O at the tetrahedral site [9]. Confirmation of the attachment of PSS onto the MNP was obtained by observing the following peaks in the spectra of (PSS-MNP): (a) an increase in intensities of bands between 3000 and 3700 $cm^{-1}$ (stretching vibration of water) and 1620 $cm^{-1}$ (O–H bending vibrations of water) in agreement with the increase in the water content in the polymeric network; (b) presence of absorption bands at 2930 and 2854 $cm^{-1}$ due to aromatic =C–H stretching vibrations and alkyl C–H stretching vibrations confirm the presence of the polyelectrolyte; (c) absence of the absorption peak at 1380 $cm^{-1}$ indicates that PSS is effective in shielding the magnetic core; (d) a decrease in intensities of absorption bands of Fe–O (stretching vibration) at 680 and 588 $cm^{-1}$ indicates chemical attachment of PSS to the MNP surface [37].

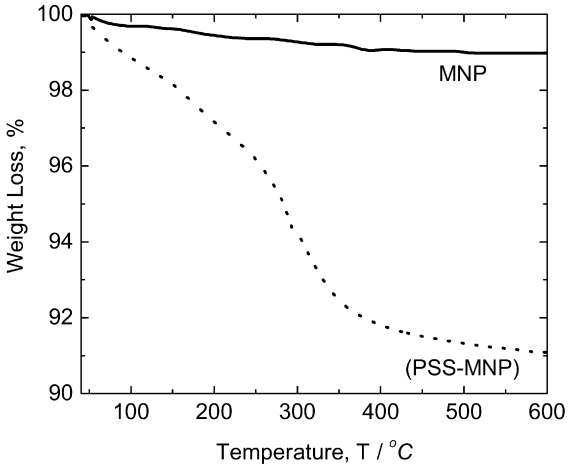


**Fig. 3.** TGA curves of positively charged MNP and negatively charged (PSS-MNP). The initial weight loss in MNP is due to evaporation of residual water, while the two-step weight loss in (PSS-MNP) is due to an initial loss of residual water followed by degradation of PSS.

The modification by PSS can be quantified by TGA as shown from the TGA curves of MNP and (PSS-MNP) in Fig. 3. As expected, the TGA curve for MNP shows no significant weight loss; the initial weight loss (at around 100–120 °C) is simply due to the evaporation of residual water. For (PSS-MNP), the initial weight loss up to about 200 °C is due to the loss of residual water in the sample and the pronounced weight loss above 200 and up to 370 °C is due to the degradation of PSS [15]. There is a minor weight loss between 370 and 600 °C, which could possibly be attributed to release of entrapped gases formed during the decomposition process. The result confirms that PSS is bound to the MNP. Fig. 3 shows pronounced weight loss (about 9%) for (PSS-MNP) and the approximate polymer content in (PSS-MNP) is estimated to be about 7–8%.

Fig. 4a shows the room temperature magnetisation loops of MNP and (PSS-MNP) in a 2 T field at 310 K. In both cases, the magnetisation curves exhibit zero coercivity and remanence indicating the superparamagnetic properties of both particles. The saturation magnetisation values of MNP and (PSS-MNP) are about 46 and 42 emu $g^{-1}$, respectively. The latter value is about twice that obtained by Flesch et al. [38] or Kamruzzaman Selim et al. [39] who reported values of 22 and 27 emu $g^{-1}$ for poly($\varepsilon$-caprolactone)- and lactobionic acid-modified MNP, respectively. (PSS-MNP) shows a (~9%) decrease in the mass magnetisation compared to the native MNP, consistent with the non-magnetic polyelectrolytes coating bound to the MNP as determined previously by TGA [15,16]. Zero-field-cooled (ZFC) and field-cooled (FC) magnetisation data (obtained from SQUID) in the temperature range of 5–300 K are shown in Fig. 4b. In the ZFC experiment, the field was set to zero and the sample was cooled down to 5 K, then the magnetisation was measured with a field of 100 Oe between 5 and 300 K. In the FC experiment, a field of 100 Oe was applied as the sample was cooled down and the magnetisation was measured when the sample was heated from 5 to 300 K in a field of 100 Oe. The ZFC curve shows a maximum $T_{max}$ at 126 K and collapses into the FC curve before the two curves separate at 250 K, which is the blocking temperature, $T_B$. Such behaviour is characteristic of superparamagnetism and is due to the progressive blocking of the magnetic moment of nanoparticles with decreasing temperature. The relatively large difference in the value of $T_B - T_{max}$ and the broad maximum suggest a broad distribution of the anisotropy energy barriers for reorientation of the magnetic moments due to the broad distribution size.

Fig. 5 depicts the time-dependent temperature curves of MNP and (PSS-MNP) in a 200 kHz and 3.8 kA $m^{-1}$ ac magnetic field.

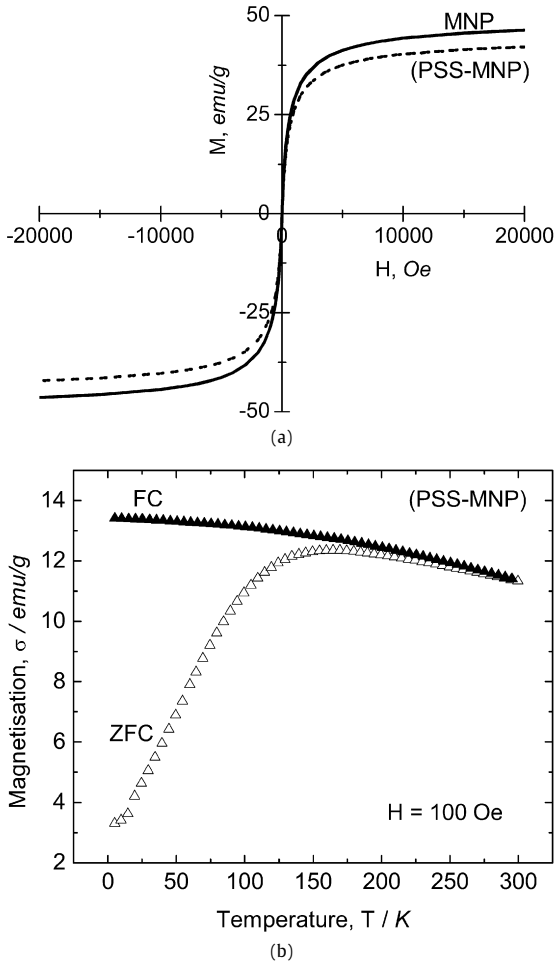


**Fig. 4.** (a) Magnetisation curves of positively charged MNP and negatively charged (PSS-MNP) exhibit zero coercivity and remanence indicating the superparamagnetic nature of both particles. (b) Temperature dependence of magnetisation of (PSS-MNP) at ZFC and FC conditions indicates the blocking temperature, $T_B \sim 250$ K.

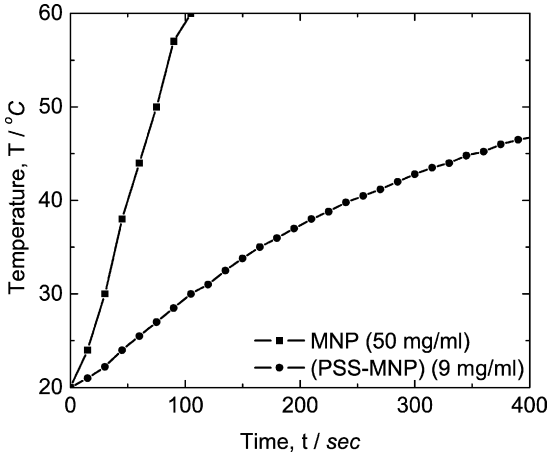


**Fig. 5.** Time-dependent temperature curves of positively charged MNP and negatively charged (PSS-MNP) in a 200 kHz and 3.8 kA $m^{-1}$ ac magnetic field show that sufficient heat is produced within a short time frame, even at low concentrations.

Under the selected field parameters, sufficient heat is produced which leads to a substantial temperature increase within a short time frame, even for dilute solutions. When MNP and (PSS-MNP) are subjected to an ac magnetic field, the magnetic particles transform the energy of the ac magnetic field into heat dominantly due to Néel relaxation. The transformation efficiency depends strongly

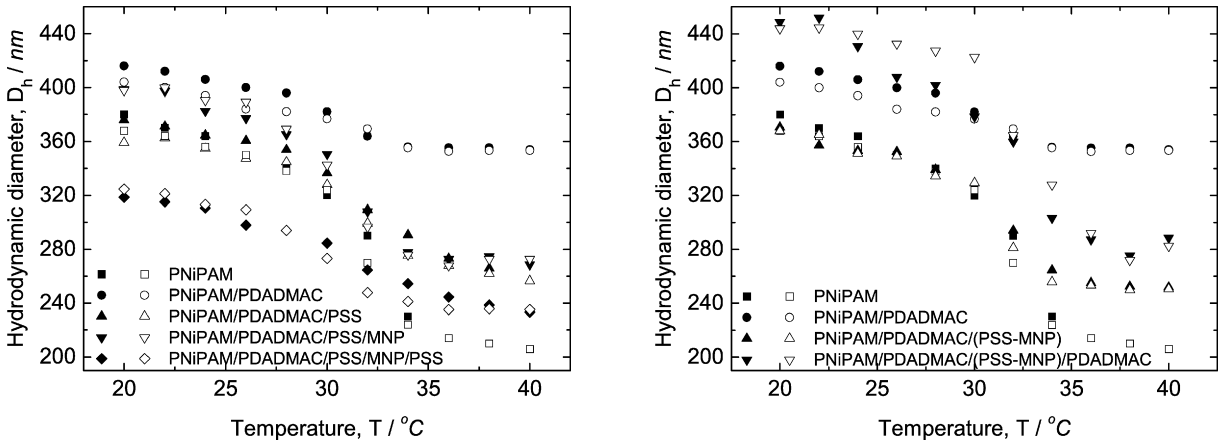


**Fig. 6.** The dependence of the hydrodynamic radius (as followed by DLS) of the hybrid core–shell PNiPAM microgel coated with polyelectrolytes and (a) MNP or (b) (PSS-MNP) as a function of temperature. Closed and open symbols represent the heating and the cooling cycle, respectively.

on the frequency of the external field as well as the nature of the particles such as magnetism and surface modification [15,40]. The specific absorption rate (SAR) was calculated using the formula

$$\mathrm{SAR} = C\frac{\Delta T}{\Delta t}\frac{1}{m_{\mathrm{Ferrite}}},$$

where $\Delta T/\Delta t$ is the initial slope of the curve, $m_{\mathrm{Ferrite}}$ is the mass of ferrite and $C$ is the specific heat capacity of the solution. Here, $C = 0.937\ \mathrm{J(g^{-1}K^{-1})}$ for ferrofluids and $C = 4.18\ \mathrm{J(g^{-1}K^{-1})}$ for water. The SAR values of MNP and (PSS-MNP) were calculated to be around 16 and 29 $\mathrm{W\,g^{-1}}$. The SAR value of (PSS-MNP) is almost twice that of MNP most probably because of the absorption of heat by the polymer coating which is bound to the magnetic core [15,16]. The decisive parameter when exploiting the inductive heating in combination with the thermosensitive principle is the effectiveness of heat transfer from the magnetic core (unmodified or modified by PSS) onto the thermoresponsive (loaded) microgel and the subsequent heat-triggered drug-release. The inductive heating reveals the advantages of having a polymeric coating or polymer-modified MNP surface by polyanions and polycations. The increase in polymeric content enhances the amount of heat generated by the MNP. Under the above-mentioned experimental conditions, MNP or (PSS-MNP) generate enough heat to raise the temperature above 40 °C within a few minutes—a property exploitable in association with thermoresponsive microgels with VPTT below that temperature.

### 3.2. Microgel-MNP characterisation

MNP were assembled on thermoresponsive PNiPAM microgel (MG) *via* the LbL assembly in an attempt to confer magnetic properties to the resulting hybrid core–shell structure [15]. The LbL assembly of PEM [28,30,32] and MNP [15] on the microgel was monitored by DLS and electrophoretic measurements. While DLS measures the hydrodynamic diameter, $D_h$, of the hybrid core–shell structures, the sign of the mobility, $\mu$, confirms charge reversal indicating successful LbL assembly after the deposition of each layer. Fig. 6a shows the dependence of $D_h$ of MG and subsequent LbL assembly of polyelectrolytes and positively charged MNP on MG as a function of temperature [28,30,32]. In this example, we first coated MG with PDADMAC (MG/PDADMAC), then with PSS (MG/PDADMAC/PSS), followed by positively charged MNP (MG/PDADMAC/PSS/MNP), and finally with a last layer of PSS to confine the MNP (MG/PDADMAC/PSS/MNP/PSS). MG has a $D_h$ of around 380 nm and 200 nm in the swollen and collapsed state respectively, with a VPTT around 32 °C. On addition of the first layer of PDADMAC, there is a slight increase in the size of MG/PDADMAC in the swollen state (around 420 nm). However in the collapsed state, the size of MG/PDADMAC is about 360 nm. The collapse of the microgel is hindered by the strong electrostatic interactions between the positively charged PDADMAC and the negatively charged MG, thus preventing the complete collapse of the microgel [15,28,30,32]. Upon addition of the second polyelectrolyte layer, the thermoresponsivity of MG/PDADMAC/PSS is comparable to that of the native microgel, but with a collapsed state at around 260 nm. On addition of the positively charged MNP in the third layer, DLS curve of MG/PDADMAC/PSS/MNP shows no significant change, with a $D_h$ of around 400 nm in the swollen state. To confine the MNP in this hybrid core–shell structure, a fourth layer of the negatively charged PSS is assembled to give the final structure MG/PDADMAC/PSS/MNP/PSS, which surprisingly has a $D_h$ of 320 nm and 240 nm in the swollen and collapsed state respectively [41]. It has been shown that the size of polyelectrolyte-coated microgels depends on the number of layers as well as the nature of the polyelectrolyte [30], but how MNP affect the size, hence thermoresponsive behaviour, is still not fully understood. The aim of this work is to show that one could successfully confine MNP between PEM at various positions on the microgel.

Fig. 6b shows the dependence of $D_h$ of MG and subsequent LbL assembly of polyelectrolytes and negatively charged (PSS-MNP) on MG as a function of temperature. In this case, we coated MG/PDADMAC with the negatively charged (PSS-MNP) (MG/PDADMAC/(PSS-MNP)), followed by a layer of PDADMAC to confine the MNP (MG/PDADMAC/(PSS-MNP)/PDADMAC). In the swollen state, the hydrodynamic diameter of MG/PDADMAC/(PSS-MNP) is almost identical to the size of the native MG (around 370 nm). However, careful analysis of the DLS curves at temperatures above the VPTT reveals that MG/PDADMAC/(PSS-MNP) is bigger than MG/PDADMAC. This indicates the presence and successful assembly of (PSS-MNP) onto the PDADMAC layer [15,28,30,32]. The final hybrid core–shell structure MG/PDADMAC/(PSS-MNP)/PDADMAC has a $D_h$ of 440 nm and 260 nm in the swollen and collapsed state, respectively.

From Fig. 6 it can be seen that swelling and deswelling of the hybrid core–shell structure is completely reversible and reproducible as revealed by the heating and cooling cycles during the DLS measurements. In the case of MG/PDADMAC/PSS/MNP/PSS microgel and MG/PDADMAC/(PSS-MNP)/PDADMAC microgel two heating and cooling cycles were run back-to-back. The DLS curve from the second cycle (data not shown) matched that from the first cycle revealing that MNP do not get detached after the phase

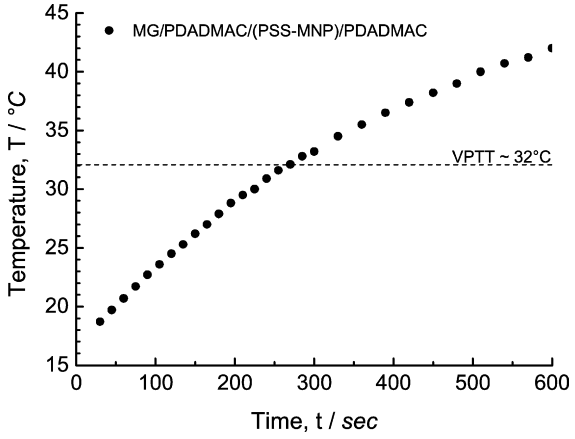


**Fig. 7.** Time-dependent temperature curve of MG/PDADMAC/(PSS-MNP)/PDADMAC microgels in a 200 kHz and 3.8 kA m$^{-1}$ ac magnetic field. The corresponding SAR calculated is around 600 W g$^{-1}$.

transition of MG during the first cycle and that the resulting hybrid core–shell systems are thermosensitive and magnetic.

The time-dependent temperature curve for MG/PDADMAC/(PSS-MNP)/PDADMAC microgel under a 200 kHz and 3.8 kA m$^{-1}$ ac magnetic field is shown in Fig. 7. Under the selected field parameters, the SAR value of MG/PDADMAC/(PSS-MNP)/PDADMAC was calculated to be around 600 W g$^{-1}$. This extremely high SAR value [42] is probably due to the absorption of heat by the microgel polymeric network as well as the polyelectrolyte multilayer coating which is bound to the magnetic core [15,16]. Even with a low content of iron, a solution of MG/PDADMAC/(PSS-MNP)/PDADMAC microgel took only between 4 to 6 min to generate enough heat to raise the temperature above the VPTT of the microgel. This low iron content and high polymeric content could be the key to high SAR values for hybrid inorganic–organic core–shell materials for hyperthermia treatment.

Fig. 8 shows the electrophoretic mobility, $\mu$, of the hybrid core–shell microgels as a function of the number of deposited layers [15]. On adsorption of the first PDADMAC layer $\mu$ of MG swings from $-1.2 \times 10^{-8}$ m$^2$ V$^{-1}$ s$^{-1}$ to $+1.3 \times 10^{-8}$ m$^2$ V$^{-1}$ s$^{-1}$ for MG/PDADMAC. Subsequent depositions of PSS, positively charged MNP and PSS (Fig. 8a) yield a $\mu$ of $-0.8 \times 10^{-8}$ m$^2$ V$^{-1}$ s$^{-1}$, $+1.5 \times 10^{-8}$ m$^2$ V$^{-1}$ s$^{-1}$ and $-4.2 \times 10^{-8}$ m$^2$ V$^{-1}$ s$^{-1}$ for MG/PDADMAC/PSS, MG/PDADMAC/PSS/MNP, and MG/PDADMAC/PSS/MNP/PSS, respectively. Similarly, depositions of negatively charged (PSS-MNP) and positively charged PDADMAC (Fig. 8b) yield a $\mu$ of $-1.8 \times 10^{-8}$ m$^2$ V$^{-1}$ s$^{-1}$ and $+1.0 \times 10^{-8}$ m$^2$ V$^{-1}$ s$^{-1}$ for MG/PDADMAC/(PSS-MNP) and MG/PDADMAC/(PSS-MNP)/PDADMAC, respectively. The $\mu$ alternates between negative and positive values corresponding to the sequential adsorption of cationic and anionic species, respectively, and thereby revealing charge overcompensation necessary for charge reversal for further build up of multilayers [15, 28,30]. One would expect a drastic charge reversal during the deposition of MNP (either positively or negatively charged) since a large amount of MNP would be required to overcompensate the charges of the underlying layer, but this is not the case. It could be that, due to strong electrostatic attractions, some of the deposited MNP find themselves buried deeper in the interdigitated layers underneath, with the result that less MNP actually contribute to the net surface charge of the ensemble. It is also interesting to point out that confining the positive MNP with a layer of negatively charged PSS leads to significant charge reversal, Fig. 8a. If this is the result of the surface behaving now like a rigid one due to the deposition of the hard MNP in the layer underneath, then one would expect also a drastic charge reversal when a PDADMAC layer is deposited on the negatively charged (PSS-MNP). However, as shown in Fig. 8b, this is not the case. It is still not clear why this sudden increase in $\mu$ (in magnitude) is observed when MNP is confined with a single layer of PSS and not when (PSS-MNP) is confined with a single layer of PDADMAC. However, if an additional layer of PSS is added to the latter system [i.e. (PSS-MNP) are confined by two outer layers of polyelectrolytes instead of one] to obtain a final hybrid core–shell structure: MG/PDADMAC/(PSS-MNP)/PDADMAC/PSS (last point in Fig. 7b where $N = 4$) a $\mu$ of around $-4.1 \times 10^{-8}$ m$^2$ V$^{-1}$ s$^{-1}$ is reached. This could be an indication that the deposition of PSS leads to a better surface coverage than that of PDADMAC as we previously reported [30].

## 4. Conclusion

We demonstrate the feasibility of independently tuning the magnetic and thermoresponsive properties of individual components, namely of magnetic nanoparticles and PNiPAM microgel, respectively, before assembling them into hybrid core–shell structures with dual-stimuli properties. We describe the synthesis and characterisation of the PNiPAM microgel, and of both positively and negatively charged magnetic nanoparticles. The layer-by-layer technique proves to be very versatile firstly in the surface modification of the PNiPAM microgel using polyelectrolytes (polyelectrolytes on microgel), secondly in the deposition of magnetic nanoparticles (nanoparticles on polyelectrolytes), and thirdly in confining these magnetic nanoparticles with another layer on polyelectrolyte (polyelectrolytes on nanoparticles). Dynamic light scattering studies show that at every stage of polyelectrolyte layering, the resulting core–shell structure retains its thermoresponsivity, and more

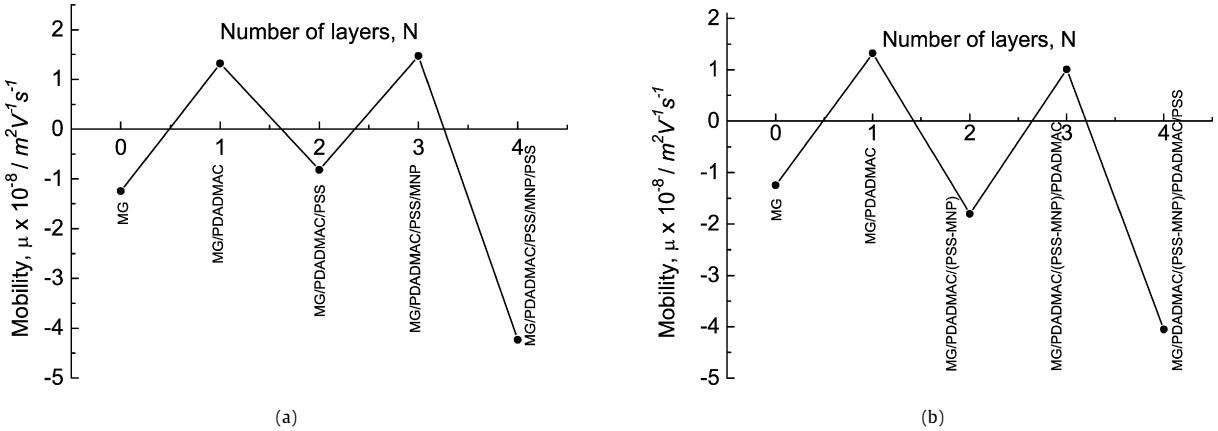


(a) (b)

**Fig. 8.** Electrophoretic measurements as a function of the number of layers assembled on the microgel using polyelectrolytes and (a) MNP (in the 3rd layer) or (b) (PSS-MNP) (in the 2nd layer) indicate successful charge reversal during the LbL deposition.

importantly, that upon deposition of magnetic nanoparticles, the resulting hybrid core–shell structure retains both thermoresponsive and magnetic properties and the nanoparticles do not get detached after the phase transition. Electrophoretic measurements show charge reversal after each layer is deposited which is a clear indication of successful deposition. Inductive heat study reveals that the heat generated by the magnetic nanoparticles is high enough to cause the collapse of the microgel above its volume phase transition temperature. These hybrid core–shell microgels possess a unique combination of thermoresponsivity and magnetism with high specific absorption rate which could open up novel prospects for remotely controlled drug carriers.

## Acknowledgments

A.K.G. would like to thank the Deutscher Akademischer Austauschdienst (DAAD) for a scholarship. Prof. H. Lueken is thanked for ZFC and FC measurements and Dr. M. Hodenius is thanked for induction heating measurements. Support by the Fonds der Chemischen Industrie (Germany) and the Department of Science and Technology (Government of India) are gratefully acknowledged.

## References

[1] L.M. Liz-Marzan, M. Giersig, P. Mulvaney, Langmuir 12 (1996) 4329–4335.
[2] F. Caruso, R.A. Caruso, H. Möhwald, Science 282 (1998) 1111–1114.
[3] F. Caruso, H. Möhwald, Langmuir 15 (1999) 8276–8281.
[4] F. Caruso, Adv. Mater. 13 (2001) 11–22.
[5] E. Bourgeat-Lami, J. Nanosci. Nanotechnol. 2 (2002) 1–24.
[6] H.P. Yap, J.F. Quinn, S.M. Ng, J. Cho, F. Caruso, Langmuir 21 (2005) 4328–4333.
[7] U. Häfeli, W. Schütt, J. Teller, M. Zborowski, Scientific and Clinical Applications of Magnetic, Plenum, New York, 1997.
[8] Q.A. Pankhurst, J. Conolly, S.K. Jones, J. Dobson, J. Phys. D Appl. Phys. 36 (2003) R167–R181.
[9] P. Tartaj, M.P. Morales, S. Veintemillas-Verdaguer, T. González-Carreo, C.J. Serna, J. Phys. D Appl. Phys. 36 (2003) R182–R197.
[10] O.V. Salata, J. Nanobiotechnol. 2 (2004) 3.
[11] A.K. Gupta, M. Gupta, Biomaterials 26 (2005) 3995–4021.
[12] T. Neuberger, B. Schoepf, H. Hofmann, M. Hofmann, B. von Rechenberg, J. Magn. Magn. Mater. 293 (2005) 483–496.
[13] M.H. Liao, D.H. Chen, J. Mater. Chem. 12 (2002) 3654–3659.
[14] P.S. Haddad, E.L. Duarte, M.S. Baptista, G.F. Goya, C.A.P. Leite, R. Itri, Prog. Colloid Polym. Sci. 128 (2004) 232–238.
[15] J.E. Wong, A.K. Gaharwar, D. Müller-Schulte, D. Bahadur, W. Richtering, J. Magn. Magn. Mater. 311 (2007) 219–223.
[16] J.E. Wong, A.K. Gaharwar, D. Müller-Schulte, D. Bahadur, W. Richtering, J. Nanosci. Nanotechnol. (2008), in press.
[17] C. Alexiou, R.J. Schmid, R. Jurgons, M. Kremer, G. Wanner, C. Bergemann, E. Huenges, T. Nawroth, W. Arnold, F.G. Parak, Eur. Biophys. J. 35 (2006) 446–450.
[18] C. Alexiou, R. Jurgons, G. Seliger, H. Iro, J. Nanosci. Nanotechnol. 6 (2006) 2762–2768.
[19] A. Jordan, P. Wust, R. Scholz, B. Tesche, H. Fähling, T. Mitrovics, T. Vogl, J. Cervos-Navarro, R. Felix, Int. J. Hyperthermia 12 (1996) 705–722.
[20] A. Jordan, R. Scholz, P. Wust, H. Schirra, T. Schiestel, H. Schmidt, R. Felix, J. Magn. Magn. Mater. 194 (1999) 185–196.
[21] A. Jordan, R. Scholz, P. Wust, H. Fähling, R. Felix, J. Magn. Magn. Mater. 201 (1999) 413–419.
[22] D. Müller-Schulte, T. Schmitz-Rode, J. Magn. Magn. Mater. 302 (2006) 267–271.
[23] T. Gelbrich, M. Feyen, A.M. Schmidt, Macromolecules 39 (2006) 3469–3472.
[24] A.M. Schmidt, Colloid Polym. Sci. 285 (2007) 953–966.
[25] R.H. Pelton, P. Chibante, Colloids Surf. 20 (1986) 247–256.
[26] G. Decher, Science 277 (1997) 1232–1237.
[27] G. Decher, J. Schmitt, Prog. Colloid Polym. Sci. 89 (1992) 160–164.
[28] N. Greinert, W. Richtering, Colloid Polym. Sci. 282 (2004) 1146–1149.
[29] R. Veyret, C. Pichot, Th. Delair, A. Elaissari, Curr. Org. Chem. 9 (2005) 1099–1106.
[30] J.E. Wong, W. Richtering, Prog. Colloid Polym. Sci. 133 (2006) 45–51.
[31] B.G. De Geest, C. Dejugnat, E. Verhoeven, G.B. Sukhorukov, A.M. Jonas, J. Plain, J. Demeester, S.C. De Smedt, J. Controlled Release 116 (2006) 159–169.
[32] J.E. Wong, C.B. Müller, A. Laschewsky, W. Richtering, J. Phys. Chem. B 111 (2007) 8527–8531.
[33] M. Karg, I. Pastoriza-Santos, J. Pérez-Juste, T. Hellweg, L.M. Liz-Marzán, Small 3 (2007) 1222–1229.
[34] R. Massart, IEEE Trans. Magn. 17 (1981) 1247–1248.
[35] H. Senff, W. Richtering, J. Chem. Phys. 111 (1999) 1705–1711.
[36] H. Senff, W. Richtering, Colloid Polym. Sci. 278 (2000) 830–840.
[37] L. Li, R.Z. Ma, N. Iyi, Y. Ebina, K. Takada, T. Sasaki, Chem. Commun. (2006) 3125–3127.
[38] C. Flesch, E. Bourgeat-Lami, S. Mornet, E. Duguet, C. Delaite, P. Dumas, J. Polym. Sci. A Polym. Chem. 43 (2005) 3221–3231.
[39] K.M. Kamruzzaman Selim, Y.S. Ha, S.J. Kim, Y.M. Chang, T.J. Kim, G.H. Lee, I.K. Kang, Biomaterials 28 (2007) 710–716.
[40] M. Ma, Y. Wu, J. Zhou, Y. Sun, Y. Zhang, N. Gu, J. Magn. Magn. Mater. 268 (2004) 33–39.
[41] J. Rubio-Retama, N.E. Zafeiropoulos, C. Serafinelli, R. Rojas-Reyna, B. Voigt, E. Lopez Cabarcos, M. Stamm, Langmuir 23 (2007) 10280–10285.
[42] S. Mornet, S. Vasseur, F. Grasset, E. Duguet, J. Mater. Chem. 14 (2004) 2161–2175.